trolled clinical trial.

Design

Two groups, a low-dose and high-dose bFGF group, have been set (**Figure 1**). In the initial step (Step 1), three patients will be enrolled in the low-dose group. After confirming the safety in the low-dose group, patients will be randomized to the low-dose or high-dose bFGF group in Step 2. Randomization-based comparison between dose groups can achieve significant improvements in accuracy and lack of bias. This comparison can provide useful information for designing and conducting future trials.

Setting and participants

This study is being conducted at Kyoto University Hospital. Patients with chronic skin ulcers are referred by physicians and also identified through a number of wound care clinics in Kyoto Prefecture and surrounding prefectures.

Inclusion criteria

1). Patients aged 20 years or older at informed consent. 2). Presence of chronic skin ulcers as below: not healing for at least 4 weeks with conventional treatments; skin graft is not expected to take; can be completely covered by a 70 mm × 100 mm device. 3). If chronic skin ulcers are present on lower extremities, the skin perfusion pressure must be ³ 30 mmHg at a site proximal or distal to those ulcers. 4). Written informed consent.

Exclusion criteria

1). Have any of the following systemic diseases: uncontrolled diabetes mellitus (defined by HbA1c ³ 10%) according to latest laboratory data obtained within 28 days before registration); requiring continued use of oral corticosteroid therapy (> 20 mg/day prednisolone equivalent); a history of malignant tumor with disease-free interval of 5 years or less. 2). Have a history of allergy to porcine-derived products, collagen, gelatin, bFGF, anesthetic drugs, disinfectants, etc. 3). Have participated in another clinical trial/study within the past three months. 4). Have participated in this study previously. 5). Women meeting any of the following: do not agree to avoid pregnancy during the study; currently pregnant or possibly pregnant; currently breastfeeding. 6). Other patients judged by the investigator or sub-investigator to be inappropriate as a subject of this study.

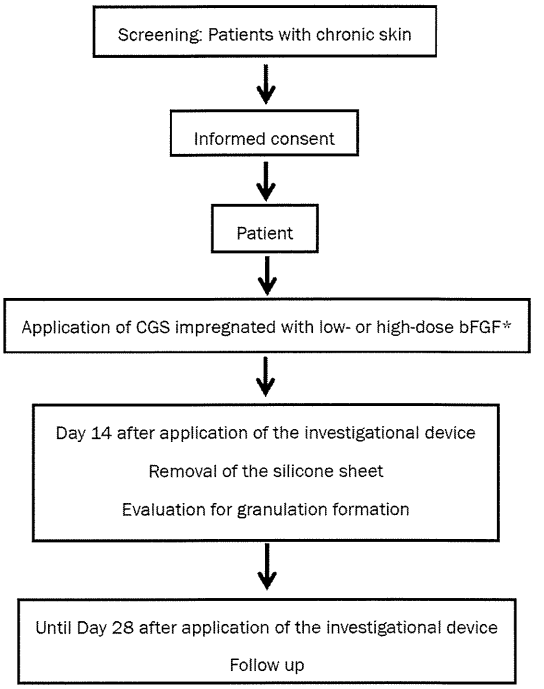

*: Step 1 (non-randomized): low-dose bFGF (n=3); Step 2 (randomized): low-dose bFGF (n=7) and high-dose bFGF (n=7)

Randomization

In Step 2, patients will be randomized to either the low-dose or high-dose bFGF group at a ratio of 1:1 without stratification. Randomization will be performed using a computer-generated random sequence to ensure equal allocation to the two dose groups by a statistician of the independent data center (Department of Clinical Trial Design and Management, Translational Research Center, Kyoto University Hospital).

Interventions

Preparations of CGS impregnated with bFGF

CGS is the modification of conventional bilayered artificial dermis (Pelnac; Gunze Co., Ltd, Kyoto, Japan) and consists of an upper silicone sheet (0.1mm in thickness) and lower sponge (3 mm in thickness) [20]. In this study, the lar-

ger CGS (82 mm × 120 mm) will be used. Two different dose bFGF concentrations of 7 μg/cm^2 (low dose) or 14 μg/cm^2 (high dose) will be used. On the day of study therapy, the investigator or sub-investigator will prepare CGS impregnated with bFGF in the operating room

Application of CGS impregnated with bFGF

This therapy will be started within 28 days of enrollment. After debridement of the chronic skin ulcers, CGS impregnated with bFGF of 7 μg/cm^2 or 14 μg/cm^2 and cut according to the shape of the wound will be applied and sutured to surrounding skin.

Dressing changes and silicone sheet removal

After the application of CGS, dressings will be changed as necessary. Patients will be hospitalized until Day 7 to ensure stabilization of the applied CGS and may be discharged on Day 8 after application according to the condition of the wound. On Day 14 after application, the sutures and silicone sheet of CGS will be removed. After silicone film removal, subsequent therapy may be started.

Subsequent therapy

The use of bFGF or another collagen-based artificial skin will be prohibited until Day 28 after application. The use of ointments, wound dressings and skin grafting will be allowed. After completion of the study period (Day 29 after investigational device application and onward), no particular restrictions will be imposed.

Digital photograph for healing assessment

Using a digital camera, digital images of the wounds will be taken with a calibrator (CASMATCH; BEAR Medic Corp., Tokyo, Japan) placed on the skin adjacent to the wound. The color and size of image will be adjusted using the CASMATCH and image editing software (Adobe Photoshop; Adobe Systems) to assess the wound and granulation areas. As with the primary endpoint, the granulation tissue evaluation committee members will assess the wound and granulation areas.

Primary endpoint

The primary endpoint is "wound bed improvement."

Granulation tissue is wound connective tissue, which forms at the beginning of wound healing [26]. This highly fibrous tissue is usually pink because numerous small capillaries invade granulation tissue to supply oxygen and nutrients. The appearance of granulation tissue is a good sign of healing because when a wound starts granulating, it means that the healing process of the wound is starting [26-28]. The area of granulation tissue will be measured as the granulation formation area in this study. An unhealed area is defined as an area with no epithelialization and no granulation formation. In this study, the percentage of wound bed improvement is defined as the value (%) calculated from the sum of the granulated and epithelialized areas on Day 14 divided by the baseline wound area after debridement on Day 0 multiplied by 100, and the patient is diagnosed with wound bed improvement if the wound bed improvement indicator is 50% or higher. The use of 50% or more as the cutoff for the wound bed improvement indicator is based on the pressure ulcer healing assessment scale by the Japanese Society of Pressure Ulcers [28, 30, 31].

Secondary endpoints

1). Adverse events and adverse reactions. 2). Percentage of "wound bed improvement". 3). Percentage of wound reduction: The percentage of wound area reduction is defined as the value (%) calculated from the wound area of the ulcer on Day 14 divided by the baseline wound area after debridement on Day 0 multiplied by 100. 4). Percentage of granulation area: The percentage of granulation area is defined as the value (%) calculated from the granulation area divided by the wound area on Day 14 multiplied by 100.

Blinding

The baseline wound area, the wound area on Day 14 and the granulation area on Day 14 will be independently measured under blinding by central review. Patients will be unblinded, and unblinded investigators will apply CGSs and change dressings.

Sample size

This study will be conducted to determine whether CGS impregnated with bFGF is promising for the treatment of chronic skin ulcers, as evaluated based on wound bed improvement as

Table 1. Schedule of study assessments and evaluations

		Treatment			Observation
Clinical assessments, testing and investigations	Day of enrollment	Day of application/ reapplication	← →	Day of silicone sheet removal (Day 14)	Day 28 after application/ reapplication
Clinical history	○				
Physical examination	○				
Eligibility criteria check	○				
Informed consent	○				
Blood test	○			○	○
Skin perfusion pressure	○				
Investigational device application		○			
Clinical assessment of the wound	○	○		○	○
Digital photograph of wound	○	○		○	○
Wound evaluation				●	
Data submission of treatment and AE etc.		○		○	○
Observation of AE		○	← ○ →	○	○

○: required; ●: Wound area measurements, granulation area measurements (wound for efficacy evaluation and wounds for study therapy)

the primary endpoint. Primary analyses will be conducted using all data treated with CGS in Step 1 and Step 2. Since debridement and conventional therapies rarely lead to wound bed improvement in this patient population, the null hypothesis tested in this study is that the proportion of patients with wound bed improvement is 10% or less. The null hypothesis is also supported by previous trials [32-34]. In consideration of the minimum clinically important difference, the expected proportion of patients with wound bed improvement in this study is set to 50% or more. When exact testing based on binomial distribution is conducted with a one-sided significance level of 2.5% and a statistical power of 90% or higher, the required number of subjects is 14. Allowing for a drop-out rate of 20% or less, the total number of patients for registration is 17, specifically 3 patients in Step 1 and 14 patients in Step 2.

Study schedule

The schedule of study assessments and evaluations is shown in **Table 1**. The study period will be from the day of informed consent to 28 days after investigational device application. The study period will be from the day of investigational device application to 28 days after investigational device application. Data to evaluate the efficacy and safety of this study will be collected at enrollment, baseline, and Day 14 of the treatment phase and Day 28 of the observation phase.

Statistical analysis

Patients who have been registered for the study and who have undergone investigational device application at least once will be included in the full analysis set (FAS) and the safety analysis

set. From the FAS, however, patients will be excluded if they have serious protocol violations or International Conference on Harmonization Guidelines for Good Clinical Practice (ICH-GCP) violations (failure to obtain consent, major study procedure violations) or if they are found to be ineligible after registration.

Wound bed improvement

Wound bed improvement is the primary endpoint of this study. The primary analysis will be conducted for the FAS using exact test based on binomial distribution with a null proportion of 10% and a one-sided significance level of 2.5%. The 95% confidence interval of the proportion of patients with wound bed improvement will be calculated using an exact method based on binomial distribution.

Percentage of wound bed improvement, would reduction and granulation area

Using the FAS, the descriptive statistics will be calculated. The interval estimation will be conducted under the assumption that this endpoint follows normal distribution.

Adverse events related to the application of the device

Using the safety analysis set, the frequency/incidence of adverse events and adverse events that can be causally related to the investigational device in the safety analysis set will be calculated by event and severity.

Ethical considerations

This study is being conducted in compliance with the ICH-GCP and in agreement with the latest revision of the Declaration of Helsinki, Pharmaceutical Affairs Law and all applicable Japanese laws and regulations, as well as any local laws and regulations and all applicable guidelines. This protocol and any amendments have Institutional Review Board approval at Kyoto University Hospital.

Subject consent

Informed consent will be obtained from all potential study participants using the IRB-approved informed consent form. The clinical investigator informs the potential study subject of all pertinent aspects of the study. The subject must sufficiently understand the contents of the information form before providing written consent. The consent form must be dated and signed by both the investigator and the participant. Subjects are also informed that their medical care will not be affected if they do not choose to participate in this study. The consent form will be retained at Kyoto University Hospital and the information form and a copy of the consent form will be handed to the participant. Whenever the investigator obtains information that may affect the participant's willingness to continue participation in the study, the investigator or sub-investigator will immediately inform the participant and record this, and reconfirm the participant's willingness to continue participation in the study.

Adverse events

This study is being conducted according to the ICH-GCP. Adverse events and serious adverse events information will be documented according to the Medical Dictionary for Regulatory Activities (MedDRA) version 14.0.

Results and discussion

This study has been designed to address the safety and efficacy of novel treatment for chronic skin ulcers using a modified artificial dermis, CGS, that can sustain bFGF. This study will be the first randomized controlled trial to evaluate the efficacy of CGS and the appropriate concentration of bFGF impregnation for treatment of increasing non-healing ulcers. Some bioengineered skin substitutes that provide growth factors secreted by living cells have been reported to be effective for chronic skin ulcers, although they are costly and access is limited to only a few areas and countries. Both CGS and bFGF are freeze-dried and can be kept well and stored at room temperature. These are off-the-shelf products and the procedure of impregnation is simple; therefore, we can use this combination therapy anywhere when needed. If successful, this intervention may lead to substantial and important changes in the management of chronic skin ulcers, such as diabetes ulcers and venous leg ulcers

Acknowledgements

This work was supported by a grant from the

Japan Science and Technology Agency.

Address correspondence to: Dr. Naoki Morimoto, Department of Plastic and Reconstructive Surgery, Graduate School of Medicine, Kyoto University, 54, Kawahara-cho Shogoin, Sakyo-ku, Kyoto 606-8507, Japan Tel: +81-75-751-3613; Fax: + 81-75-751-4340; E-mail: mnaoki22@kuhp.kyoto-u.ac.jp

References

[1] Vuorisalo S, Venermo M, Lepäntalo M. Treatment of diabetic foot ulcers. J Cardiovasc Surg (Torino) 2009; 50: 275-291.

[2] Bergqvist D, Lindholm C, Nelzen O. Chronic leg ulcers: the impact of venous disease. J Vasc Surg 1999; 29: 752-755.

[3] Singh N, Armstrong DG, Lipsky BA. Preventing foot ulcers in patients with diabetes. JAMA 2005; 293: 217-228.

[4] Wu SC, Driver VR, Wrobel JS, Armstrong DG. Foot ulcers in the diabetic patient, prevention and treatment. Vasc Health Risk Manag 2007; 3: 65-76.

[5] Ehrenreich M, Ruszczak Z. Update on tissue-engineered biological dressings. Tissue Eng 2006; 12: 2407-2424.

[6] Mason C, Manzotti E. Regenerative medicine cell therapies: numbers of units manufactured and patients treated between 1988 and 2010. Regen Med 2010; 5: 307-313.

[7] Uchi H, Igarashi A, Urabe K, Koga T, Nakayama J, Kawamori R, Tamaki K, Hirakata H, Ohmura T, Furue M. Clinical efficacy of basic fibroblast growth factor (bFGF) for diabetic ulcer. Eur J Dermatol 2009; 19: 461-468.

[8] Trier WC, Peacock EE Jr, Madden JW. Studies on the effectiveness of surgical management of chronic leg ulcers. Plast Reconstr Surg 1970; 45: 20-23.

[9] Suzuki S, Matsuda K, Issiki N, Tamada Y, Ikada Y. Experimental study of a newly developed bilayer artificial skin. Biomaterials 1990; 11: 356-360.

[10] Suzuki S, Matsuda K, Isshiki N, Tamada Y, Yoshioka K, Ikada Y. Clinical evaluation of a new bilayer 'artificial skin' composed of collagen sponge and silicone layer. Br J Plast Surg 1990; 43: 47-54.

[11] Yannas IV, Orgill DP, Burke JF. Template for skin regeneration. Plast Reconstr Surg 2011; 127: 60S-70S.

[12] Yannas IV, Burke JF. Design of an artificial skin. I. Basic design principles. J Biomed Mater Res 1980; 14: 65-81.

[13] Gospodarowicz D. Localization of a fibroblast growth factor and its effect alone and with hydrocortisone on 3T3 cell growth. Nature 1974; 249: 123-127.

[14] Hom DB, Unger GM, Pernell KJ, Manivel JC. Improving surgical wound healing with basic fibroblast growth factor after radiation. Laryngoscope 2005; 115: 412-422.

[15] Akita S, Akino K, Imaizumi T, Hirano A. Basic fibroblast growth factor accelerates and improves second-degree burn wound healing. Wound Repair Regen 2008; 16: 635-641.

[16] Muneuchi G, Suzuki S, Moriue T, Igawa HH. Combined treatment using artificial dermis and basic fibroblast growth factor (bFGF) for intractable fingertip ulcers caused by atypical burn injuries. Burns 2005; 31: 514-517.

[17] Akita S, Akino K, Tanaka K, Anraku K, Hirano A. A basic fibroblast growth factor improves lower extremity wound healing with a porcine-derived skin substitute. J Trauma 2008; 64: 809-815.

[18] Ito K, Ito S, Sekine M, Abe M. Reconstruction of the soft tissue of a deep diabetic foot wound with artificial dermis and recombinant basic fibroblast growth factor. Plast Reconstr Surg 2005; 115: 567-572

[19] Fujioka M. Combination treatment with basic fibroblast growth factor and artificial dermis improves complex wounds in patients with a history of long-term systemic corticosteroid use. Dermatol Surg 2009; 35: 1422-1425.

[20] Takemoto S, Morimoto N, Kimura Y, Taira T, Kitagawa T, Tomihata K, Tabata Y, Suzuki S. Preparation of collagen/gelatin sponge scaffold for sustained release of bFGF. Tissue Eng Part A 2008; 14: 1629-1638.

[21] Kanda N, Morimoto N, Takemoto S, Ayvazyan AA, Kawai K, Sakamoto Y, Taira T, Suzuki S. Efficacy of Novel Collagen/Gelatin Scaffold With Sustained Release of Basic Fibroblast Growth Factor for Dermis-like Tissue Regeneration. Ann Plast Surg 2011. [Epub ahead of print]

[22] Ayvazyan AA, Morimoto N, Kanda N, Kawai K, Sakamoto Y, Taira T, Suzuki S. Collagen-gelatin scaffold impregnated with bFGF accelerates palatal wound healing of palatal mucosa in dogs. J Surgical Res 2011; 171: 247-257.

[23] Langer A, Rogowski W. Systematic review of economic evaluations of human cell-derived wound care products for the treatment of venous leg and diabetic foot ulcers. BMC Health Serv Res 2009; 9: 115.

[24] O'Reilly D, Linden R, Fedorko L, Tarride JE, Jones WG, Bowen JM, Goeree R. A prospective, double-blind, randomized, controlled clinical trial comparing standard wound care with adjunctive hyperbaric oxygen therapy (HBOT) to standard wound care only for the treatment of chronic, non-healing ulcers of the lower limb in patients with diabetes mellitus: a study protocol. Trials 2011; 12: 69.

[25] Wong T, McGrath JA, Navsaria H. The role of fibroblasts in tissue engineering and regeneration. Br J Dermatol 2007; 156: 1149-1155.

[26] Shaw TJ, Martin P. Wound repair at a glance. J Cell Sci 2009; 122: 3209-3213.

[27] Martin P. Wound Healing-Aiming for Perfect

Skin Regeneration. Science 1997; 276: 75-81.
[28] Sanada H, Moriguchi T, Miyachi Y, Ohura T, Nakajo T, Tokunaga K, Fukui M, Sugama J, Kitagawa A. Reliability and validity of DESIGN, a tool that classifies pressure ulcer severity and monitors healing. J Wound Care 2004; 13: 13-18.
[29] Lavery LA, Barnes SA, Keith MS, Seaman JW Jr, Armstrong DG. Prediction of healing for postoperative diabetic foot wounds based on early wound area progression. Diabetes Care 2008; 31: 26-29.
[30] Japanese Society of Pressure Ulcers. Guideline for Local Treatment of Pressure Ulcers 2005.
[31] Japanese Society of Pressure Ulcers. Guideline for Prevention and Management of Pressure Ulcers. 2009.
[32] Veves A, Falanga V, Armstrong DG, Sabolinski ML. Graftskin, a human skin equivalent, is effective in the management of noninfected neuropathic diabetic foot ulcers: a prospective randomized multicenter clinical trial. Diabetes Care 2001; 24: 290-295.
[33] Cardinal M, Eisenbud DE, Armstrong DG, Zelen C, Driver V, Attinger C, Phillips T, Harding K. Serial surgical debridement: a retrospective study on clinical outcomes in chronic lower extremity wounds. Wound Repair Regen 2009; 17: 306-311.
[34] Armstrong DG, Lavery LA. Negative pressure wound therapy after partial diabetic foot amputation: a multicentre, randomised controlled trial. Lancet 2005; 366: 1704-1710.

Eur Spine J
DOI 10.1007/s00586-011-1728-3

ORIGINAL ARTICLE

A novel synthetic material for spinal fusion: a prospective clinical trial of porous bioactive titanium metal for lumbar interbody fusion

Shunsuke Fujibayashi · Mitsuru Takemoto · Masashi Neo · Tomiharu Matsushita · Tadashi Kokubo · Kenji Doi · Tatsuya Ito · Akira Shimizu · Takashi Nakamura

Received: 6 December 2010 / Revised: 23 January 2011 / Accepted: 16 February 2011

Abstract The objective of this study was to establish the efficacy and safety of porous bioactive titanium metal for use in a spinal fusion device, based on a prospective human clinical trial. A high-strength spinal interbody fusion device was manufactured from porous titanium metal. A bioactive surface was produced by simple chemical and thermal treatment. Five patients with unstable lumbar spine disease were treated surgically using this device in a clinical trial approved by our Ethics Review Committee and the University Hospital Medical Information Network. Clinical and radiological results were reported at the minimum follow-up period of 1 year. The optimal mechanical strength and interconnected structure of the porous titanium metal were adjusted for the device. The whole surface of porous titanium metal was treated uniformly and its bioactive ability was confirmed before clinical use. Successful bony union was achieved in all cases within 6 months without the need for autologous iliac crest bone grafting. Two specific findings including an anchoring effect and gap filling were evident radiologically. All clinical parameters improved significantly after the operation and no adverse effects were encountered during the follow-up period. Although a larger and longer-term follow-up clinical study is mandatory to reach any firm conclusions, the study results show that this porous bioactive titanium metal is promising material for a spinal fusion device.

Keywords Porous titanium metal · Spinal fusion · Biomaterial · Clinical trial

S. Fujibayashi (✉) · M. Takemoto · M. Neo · T. Nakamura
Department of Orthopedic Surgery,
Graduate School of Medicine, Kyoto University,
Kyoto 606-8507, Japan
e-mail: shfuji@kuhp.kyoto-u.ac.jp

T. Matsushita · T. Kokubo
Department of Biomedical Sciences, College of Life and Health Sciences, Chubu University, Kasugai 487-8501, Japan

K. Doi
Osaka Yakin Kogyou Co.,Ltd, Miki 673-0043, Japan

T. Ito · A. Shimizu
Department of Experimental Therapeutics,
Translational Research Center,
Kyoto University Hospital, Kyoto 606-8507, Japan

Introduction

Osteoconductive synthetic materials including sintered hydroxyapatite ($Ca_{10}(PO_4)_6(OH)_2$ or HA), Na_2O-CaO-SiO_2-P_2O_5 system (Bioglass®) and glass ceramics containing apatite and wollastonite (AW-GC) are widely used clinically as bone substitutes [7, 12, 16]. Because application for load-bearing conditions such as the spine or long bones requires high mechanical strength, solid materials are usually used. However, such materials are brittle against shearing forces and bond to the surrounding bone only at their surface. Porous materials have advantages over solid materials in terms of bone bonding, because they can demonstrate both osteoconductive bonding and mechanical interlocking through bone tissue ingrowth into the pores. Conventional porous synthetic materials such as granules of HA and AW-GC have been applied clinically as bone graft expanders for lumbar posterolateral fusion or bone void fillers after tumor excision [8]. However, because of their poor mechanical strength, porous body of such materials cannot be applied in load-bearing conditions. Thus, achieving both high bone-bonding ability and high mechanical strength is quite difficult for porous

Published online: 03 March 2011

materials. To overcome this problem, we have developed porous bioactive titanium metal, which possesses both high bone-bonding ability and high mechanical strength simultaneously [24]. Titanium metal and its alloys can be changed to bioactive materials by simple chemical and thermal surface treatment [9, 18]. This can be applied to porous titanium metal as well [15]. Several experiments on animal models showed the safety and efficacy of porous bioactive titanium metal as a synthetic bone under load-bearing conditions. Our preclinical study [26] demonstrated that bioactive treatment effectively enhanced the fusion ability of the porous titanium implants in a canine model of spinal interbody fusion.

Instrumented spinal fusion with autologous iliac crest bone grafting (ICBG) is a gold-standard surgical procedure for the treatment of unstable spinal diseases. However, grafts harvested from the iliac crest are still a major source of autologous bone and the harvesting process is associated with graft site morbidities including residual pain, long operative times and significant blood loss [1].

To accelerate the fusion rate and alleviate donor site problems, several effective osteoinductive agents including recombinant human bone morphogenetic protein-2 (rhBMP-2) and osteogenic protein-1 (OP-1/BMP-7) have been introduced and are widely used clinically [3, 20]. Excellent clinical results have been documented, although some serious adverse effects (AEs) have been reported such as osteolysis around the cage implant, massive bleeding and soft tissue swelling [19, 27, 31]. Porous bioactive titanium metal is not only osteoconductive but also has osteoinductive ability without the need for additional osteogenic cells or agents [10, 25]. Although the osteoinductive ability of porous bioactive titanium metal is limited and the actual mechanism has not been clarified, the osteogenesis it induces is believed to guarantee the high osteoconductive ability of this material.

We conducted a clinical trial of porous bioactive titanium metal for lumbar interbody fusion. Here, we report our preliminary results and discuss the safety and efficacy of porous bioactive titanium metal as one of a new generation of synthetic device materials. This trial was based upon extensive experiments in animal models and clinical success in cementless total hip prosthesis using porous bioactive titanium metal [14, 26].

Methods

Preparation of porous implants

Porous titanium metal was manufactured from a mixture of commercially pure titanium powder <45 μm in particle size (Osaka Titanium Tech. Co. Ltd, Osaka, Japan) and ammonium hydrogen carbonate as spacer particle [32]. Sintering was carried out at 1,400°C for 2 h in Argon gas. Three types of implants, 7, 8 and 9 mm thick and 30 mm wide, were prepared for the clinical trial (Fig. 1). To improve the safety of handling during surgery, a thin outer frame was placed around the porous body and sintered. These implants were supplied by Osaka Yakin Co. (Osaka, Japan). Micro-computed tomography (CT) analysis demonstrated that more than 99% of the porous structures were interconnected and more than 80% of pores were connected through channels more than 52 μm in diameter (Fig. 2). The average porosity was 60% and the average pore size was 250 μm.

Mechanical properties of the porous titanium implants

The compressive strength of the porous titanium body was measured using a universal testing machine (Model EHF-LV020K1-010, Shimadzu Corp., Kyoto, Japan) at a cross-head speed of 1 mm/min. 0.2% yield compressive strength and Young's modulus of a typical 60% porous body were

Fig. 1 Photograph of porous bioactive titanium device for transforaminal lumbar interbody fusion

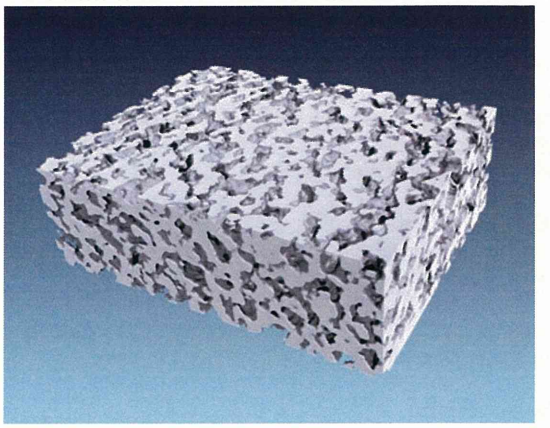

Fig. 2 Micro-computed tomography image showing well-connected internal porous structures

53.0 MPa and 4.2 GPa, respectively. The stiffness was 91.5 kN/m, and this increased to 458.3 kN/m at the outer frame. The porous body combined with the outer frame proved stable against a cyclic load of 10,000 N at 4 Hz for 1,000,000 cycles.

Bioactive surface treatment

The porous implants were treated chemically and thermally to give them a bioactive surface, as described [9, 18]. Briefly, the sintered porous titanium bodies were immersed in 5 M aqueous NaOH solution at 60°C for 24 h, 0.5 mM HCl at 40°C for 24 h, ultrapure water at 40°C for 24 h and then heat-treated at 600°C for 1 h. The homogeneity of the bioactive surface was confirmed by examining the topography and the chemistry of the center and the peripheral parts of several implants using a field emission scanning electron microscope (FE-SEM; Hitachi S-4300, Ibaraki, Japan), an energy-dispersive X-ray microanalyzer (EDX) and X-ray diffractometry (XRD). In vitro apatite-forming ability was confirmed by soaking samples for 3 days in an acellular simulated body fluid (SBF) with ion concentrations (in mM) of Na^+ 142.0, K^+ 5.0, Mg^{2+} 1.5, Ca^{2+} 2.5, Cl^- 147.8, HCO_3^- 4.2, HPO_4^{2-} 1.0 and SO_4^{2-} 0.5: nearly equal to those of human blood plasma at 36.5°C and prerequisite conditions for generating bioactive materials [17]. The implants were sterilized by 25 kGy γ-radiology exposure before surgical implantation.

Evaluation of implants

All devices with the same lot number destined for clinical use were analyzed in vitro before implantation. All parameters of mechanical strength including yield compressive strength, elastic modulus and fatigue strength were within an error of <5%. Mechanical testing found no failure of the device, nor any loss of titanium particles. FE-SEM, EDX and XRD studies confirmed the homogeneity of the bioactive surface both centrally and peripherally. After the surface treatment, the whole porous surface was uniformly changed to a bioactive thin TiO2 layer approximately 1 μm thick with sub-micron-sized pores. The walls of the porous body were completely covered with apatite within 3 days of soaking in SBF, indicating that the whole surface of the implant could be rendered bioactive by the chemical and thermal treatments (Fig. 3a–c).

Transforaminal lumbar interbody fusion (TLIF) [11]

All surgical procedures were performed by the two senior authors (S.F. and M.T.).

Following a midline skin incision, the lateral aspect of facet joints was exposed through a midline subperiosteal approach or Wiltse's approach depending on the case. After bilateral pedicle screw placement, the neural foramen was exposed by excision of the ipsilateral facet joint. Disc space preparation with the removal of degenerative disc materials and cartilaginous endplate was performed carefully from the safety triangle zone between the exiting and traversing nerve roots. In the case of concomitant spinal canal stenosis, neural decompression was done using a surgical microscope. The bioactive porous titanium implant was placed into the intervertebral space through the opened safety triangle zone and small local bone chips were packed around the implant as monitoring bone material. Compressive force was applied through the pedicle screws and pre-bent rods were set on the screws bilaterally. The patients were allowed to walk while wearing a hard brace beginning on the first day after surgery.

Patients

This was a prospective clinical case series on five patients (3 men and 2 women) with degenerative unstable lumbar

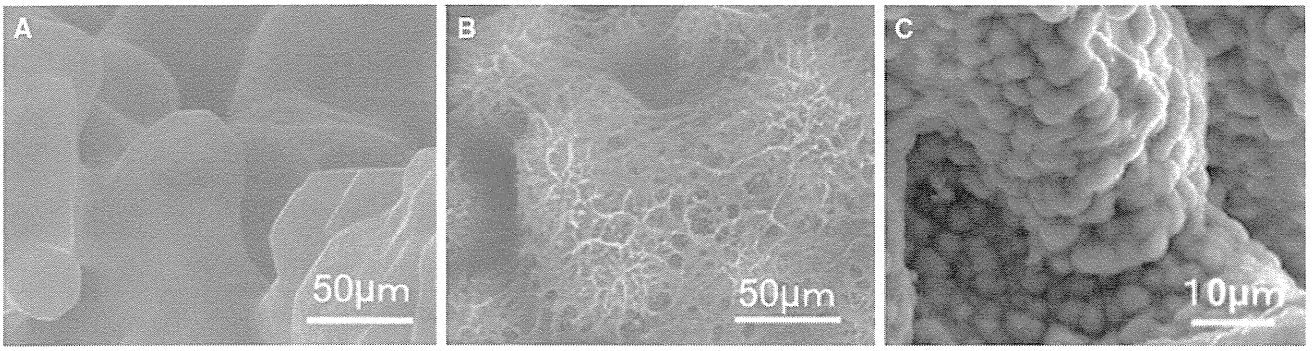

Fig. 3 Field emission scanning electron microscope (FE-SEM) images showing surface morphological changes to the porous titanium metal. **a** Before treatment, the surface was smooth. **b** After chemical and thermal treatment, a thin submicron-sized pore layer was formed on the surface. **c** Apatite formation on the whole surface of the porous bioactive titanium metal after soaking in simulated body fluid (SBF) for 3 days

lesion who were eligible for surgical treatment and who were referred to our University Hospital from November 2008 to June 2009. In all cases, the patient and his or her relatives were informed about the benefits and the risks of the implant. Written informed consent was obtained from all patients and/or their relatives, in accordance with protocols approved by our Institutional Ethics Committee and in agreement with the Declaration of Helsinki.

Among the five patients enrolled there were three with degenerative spondylolisthesis and two with isthmic spondylolisthesis. Inclusion criteria for this preliminary clinical trial were symptomatic single-level unstable lumbar disc disease with or without compression of neural elements, which were refractory to adequate conservative treatments for at least 3 months preoperatively. Patients with multilevel diseases, a previously operated spine, osteoporosis, general inflammatory disease or a severe comorbidity such as cardiovascular disease or renal dysfunction were excluded. The average age of the enrolled patients at surgery was 51.6 years (range 36–61 years).

Clinical assessment

A patient self-assessed 100 mm visual analog scale (VAS) (0 mm = no pain, 100 mm = worst pain imaginable) for both low back pain (LBP) and leg pain (LP), the Japanese Orthopaedic Association (JOA) score (Table 1) and its recovery rate [recovery rate = postoperative score − preoperative score/29 (full score) − preoperative score × 100 (%)] were examined before operation and postoperatively. A self-assessed patient's satisfaction score was examined after the surgery. For subjective assessment of the overall results of surgery, the patient was asked to select from among the options: very satisfied, satisfied, somewhat satisfied, somewhat dissatisfied or dissatisfied. The satisfaction score was recorded as a score at all time points. All patients complained of LBP preoperatively and four complained of concomitant LP. The average preoperative JOA score was 15.8 (range 11–21). The average preoperative VAS values for LBP and LP were 37.6 mm (range 10–50 mm) and 21.4 mm (range 0–60 mm), respectively. An independent expert nurse carried out the assessment of pre- and postoperative VAS and the patient's satisfaction score. The JOA scores and VAS measures were analyzed statistically using paired *t*-tests and $P < 0.05$ was considered statistically significant.

Radiological assessment

Magnetic resonance imaging (MRI), multidetector-row computed tomography (MDCT) and lateral dynamic X-rays were used to assess the neural compression and

Table 1 JOA score classifications for low-back pain

Parameter	JOA score
Subjective symptoms	9
Low-back pain	
None	3
Occasional mild pain	2
Frequent mild or occasional severe pain	1
Frequent or continuous severe pain	0
Leg pain and/or tingling	
None	3
Occasional slight symptoms	2
Frequent slight or occasional severe symptoms	1
Frequent or continuous severe symptoms	0
Gait	
Normal	3
Able to walk >500 m, although it causes pain, tingling, and/or muscle weakness	2
Unable to walk >500 m due to leg pain, tingling, and/or muscle weakness	1
Unable to walk >100 m due to leg pain, tingling, and/or muscle weakness	0
Clinical signs	6
Straight leg-raising test (including tight hamstrings)	
Normal	2
30–70°	1
<30°	0
Sensory disturbance	
None	2
Slight disturbance (not subjective)	1
Marked disturbance	0
Motor disturbance	
Normal (Grade 5/5)	2
Slight weakness (Grade 4/5)	1
Marked weakness (Garde 0–3/5)	0
Restriction of ADL	14
ADL (restriction)	
Turning over while lying down	
Standing	
Washing	
Leaning forward	
Sitting (~1 h)	
Lifting/holding heavy objects	
Walking	
Urinary bladder function	−6
Normal	0
Mild dysuria	−3
Severe dysuria (incontinence, urinary retention)	−6

JOA Japanese Orthopaedic Association

ADL activities of daily living

For each activity of daily living category severe restriction was accorded a score of 0; moderate restriction, a score of 1; and no restriction, a score of 2

dynamic situation. Preoperative dynamic lateral X-rays showed marked segmental instability in all five patients. To assess bony union postoperatively, lateral dynamic radiographs were obtained at 3, 6 and 12 months. More than 3° motion on flexion–extension was considered to indicate nonunion. In addition, radiolucent regions around the pedicle screws and the implant were defined as showing nonunion. To evaluate the placement of implant and pedicle screws, bony union and AEs, coronal and sagittal reconstruction views using MDCT were assessed at 1 week and at 1, 3, 6 and 12 months after surgery. Bony union was defined as complete when there was osseous continuity between bony endplate and implant on both the coronal and sagittal MDCT images. Nonunion was defined as the presence of a visible gap between the vertebral endplate and implant, or radiolucency around the pedicle screws. Successful bony union was recorded when the assessments of aforementioned radiological parameters were complete. A change of 3 mm or more of implant migration into the vertebral endplate was defined as significant subsidence. MRI was performed at 1 week and at 1, 3, 6 and 12 months after surgery to assess neural decompression and dural tube extension, any AEs including inflammatory reaction around the implant such as vertebral endplate erosion, Modic change [20] and any fluid collection. Three independent experienced spinal surgeons, each with at least 10 years of experience, did all the radiological assessments. Each patient's preoperative clinical and radiological data are summarized in Table 2.

Ethical considerations

The study was performed in accordance with the principles of the Declaration of Helsinki and of Good Clinical Practice and was registered on the University Hospital Medical Information Network Clinical Trials Registry (UMIN00000 1448). Approval was obtained from the relevant competent authorities and our institutional Committee of Ethics before the trial began. As clinicians, the authors played a leading role in this new type of clinical trial, which is extremely rare in the development of new medical devices in Japan. We prepared all the protocols of this study by ourselves and were supported by a translational research center in Kyoto University. The independent clinical research coordinator of the translational research center managed all clinical data, which were extracted from each patient's clinical research form. The endpoints of this clinical trial were achievement of good clinical results, bony union, no serious AEs and avoidance of the need for autologous ICBG.

Results

Clinical results

In all five patients, the preoperative LBP and radicular symptoms were resolved immediately after the operation. No surgery-related neurological deficit or wound breakdown was observed in any patient. The mean operating time was 164.6 min (range 154–179 min) and the mean estimated intraoperative blood loss was 192 mL (range 80–310 mL). No patient required transfusion or ICBG. No surgery-related complication was observed. The mean follow-up period was 15.2 months (range 12–19 months). The average postoperative JOA score was 25.6 at 1 month, 25.6 at 3 months, 27 at 6 months and 26.6 at 12 months (range 18–29). The mean recovery rate of the JOA score was 76.6% at 1 month, 77.5% at 3 months, 88.0% at 6 months and 85.8% at 12 months (range 38.9–100%). The postoperative JOA score improved significantly compared with the preoperative score at all times ($P = 0.002$ at 12 months). The mean VAS was 2 mm at 1 month, 2 mm at 3 months, 6 mm at 6 months and 2 mm at 12 months (range 0–30 mm) for LBP. It was 0 mm at 1 month, 0 mm at 3 months, 4 mm at 6 months and 2 mm at 12 months (range 0–20 mm) for LP. Both VAS measures were significantly improved compared with preoperative scores at all times (at 12 months; LBP $P = 0.027$; LP $P = 0.012$). All but one patient satisfied very much through the experiment periods. All clinical parameters showed rapid recovery within 1 month, which indicated a low level of invasiveness and good stabilization of the surgery (Fig. 4).

Table 2 Summary of preoperative patient's demographic data

Case	Age	Sex	Diagnosis	Level	Symptoms	Pre JOA	Pre VAS (LBP)	Pre VAS (LP)
1	54	F	DS	L4/5	LBP + LP	21	10	60
2	36	M	IS	L5/S	LBP + LP	12	80	50
3	51	F	DS	L4/5	LBP	19	80	0
4	61	F	DS	L4/5	LBP + LP	11	60	60
5	56	M	IS	L5/S	LBP + LP	16	50	20

DS degenerative spondylolisthesis, *IS* isthmic spondylolisthesis, *LP* leg pain, *LBP* low back pain, *VAS* visual analog scale

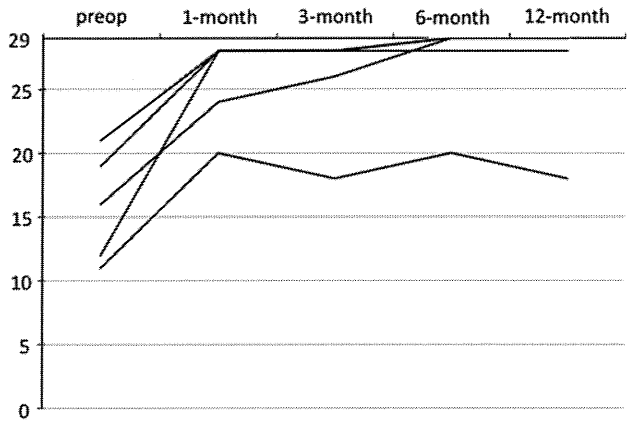

Fig. 4 Sequential changes in the Japan Orthopaedic Association (JOA) score of the five cases. The graph indicates a rapid recovery of the patients' clinical status within 1 month

Radiological results

Dynamic radiological examination showed a solid bony construct without abnormal segmental motion or radiolucency around the implants in all cases after 3 months. No patient exhibited significant implant subsidence during the follow-up period. Immediate postoperative MDCT demonstrated good apposition between the vertebral endplate and implant in all but one case. These findings indicated good anchoring of the porous titanium implant to the surrounding bone. Follow-up MDCT showed good bone ingrown onto the surface of the porous titanium metal without radiolucent line. It also showed remodeling not only of the monitoring bone but also of the surrounding vertebral bone. However, in Case 5, a gap was evident between porous titanium metal and surrounding vertebral endplate on the MDCT image immediately after the operation, because of a poor fit of the device surface with an irregular vertebral endplate. The gap was filled gradually and closed at the final follow-up MDCT (Fig. 5a–c).

Because the radiological parameters mentioned above were complete in all cases, bony union was considered to be achieved in all cases by 6 months after the operation. Postoperative MRI scans showed no significant AE such as abnormal fluid collection or apparent change in the Modic sign. In three patients with concomitant spinal canal stenosis, successful neural tissue decompression was also confirmed. The postoperative clinical and radiological results are summarized in Table 3.

Illustrative case (Case 1)

This 54-year-old woman had complained of LBP and intractable bilateral LP for 3 years before surgery. These were refractory to adequate conservative treatment. She also complained of an inability to walk for longer than 10 min, with intermittent claudication. A physical examination demonstrated bilateral dysesthesia on the L5 sensory dermatome. Her preoperative JOA score was 21 points and her self-reported VAS was 10 mm for LBP and 60 mm for LP. X-ray images showed degenerative spondylolisthesis at the L4–5 level with instability (Fig. 6a). Preoperative MR imaging demonstrated severe spinal canal stenosis at the L4–5 level. Transforaminal lumbar interbody fusion and spinal canal decompression using our bioactive titanium was performed. The operating time was 173 min and the estimated intraoperative blood loss was 140 mL. Immediate postoperative coronal imaging using MDCT demonstrated a press fit at the interface between the porous titanium metal and the vertebral endplate (Fig. 6b). Three months after the operation, dynamic X-ray imaging demonstrated no abnormal movement (Fig. 6c). Sagittal imaging using MDCT showed a stable interface without a radiolucent line or any clear zones around the pedicle screws, indicating a successful bony union (Fig. 6d). Postoperative MR imaging showed good neural decompression without any AEs. Her JOA score recovered to 29

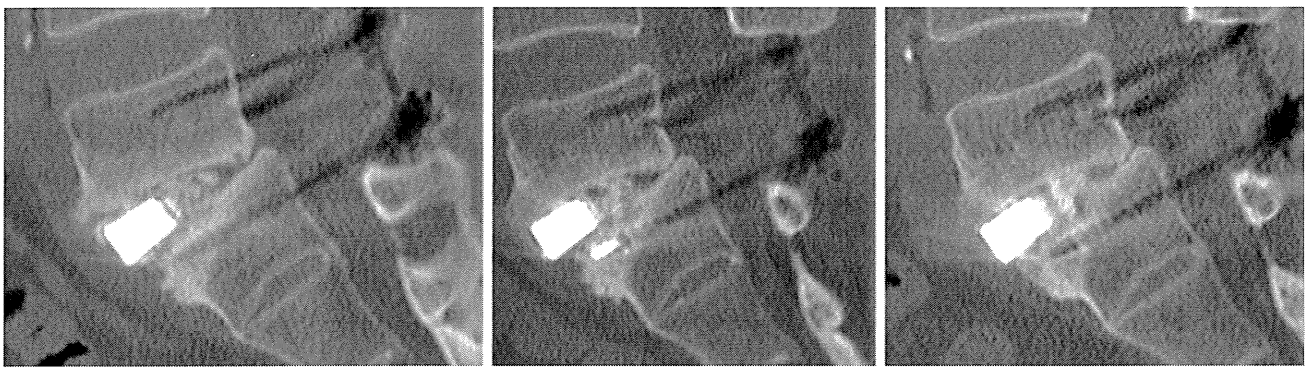

Fig. 5 Sagittal multidetector-row computed tomography (MDCT) images taken immediately postoperatively and at 3 and 12 months for Case 5. The immediate postoperative image (*left*) shows an apparent gap between the porous titanium metal and vertebral bone. The 3-month image (*center*) demonstrates bone ingrowth cranial to the porous titanium metal. The 12-month image (*right*) demonstrates complete gap filling and direct bone bonding to the porous titanium metal

Table 3 Summary of postoperative patient's demographic data

Case	Op. time (min.)	Blood loss (mL)	Post JOA score	JOA score recovery rate (%)	Post VAS (LBP)	Post VAS (LP)	Satisfaction score	ICBG	AEs	Bony union (month)
1	173	140	29	100	0	0	1	–	–	3
2	179	310	29	100	0	0	1	–	–	3
3	160	80	28	90	0	0	1	–	–	3
4	154	228	18	38.9	10	10	4	–	–	6
5	157	192	29	100	0	0	1	–	–	3

ICBG Iliac crest bone graft, *AEs* adverse effects

Satisfaction score 1, very satisfied 2, satisfied 3, somewhat satisfied 4, somewhat dissatisfied 5, dissatisfied

JOA score, VAS, and satisfaction score are obtained at 12 months after the surgery

points and the VAS score was 0 mm for LBP and 0 mm for LP at the final follow-up.

Discussion

Here, we report the safety and efficacy of porous bioactive titanium metal for the treatment of unstable lumbar disc disease. All cases showed early bony union by 6 months without autologous ICBG and rapid recovery after the surgery. The patients' satisfaction and clinical recovery rates were both acceptable.

The use of an interbody fusion cage with autologous bone grafting is a standard procedure for lumbar spinal fusion. However, nonunion, cage subsidence, implant failure and donor site morbidity are still of concern [1]. Porous materials with adequate pore structure and appropriate mechanical properties might represent an alternative to traditional cage implants. Interconnected pores permit tissue ingrowth and thus anchor the prosthesis to the surrounding bone, preventing loosening. This concept also allows a larger support area because no graft space is required and it might be effective for the prevention of implant subsidence. In the current study, significant implant subsidence has not occurred throughout the follow-up periods. Furthermore, if bone bridging can be achieved across the whole implant through the interconnected pores from one vertebra to the other it reduces the risk of implant failure and ensures long-term stability.

The kind of material and its pore characteristics influence the mechanical strength of porous biomaterials. Porous HA implants have good biocompatibility and osteoconductivity, but their mechanical properties are not adequate for load-bearing conditions. The clinical application of such conventional porous materials is limited to non-load-bearing conditions. Therefore, the use of metal to produce porous implants with higher mechanical strength is required. By using titanium metal as a starting material, our device with high porosity and large pore size acquired a high mechanical strength that is adequate for load-bearing conditions. In a previous study, we investigated the relationship between pore structure and bone ingrowth in vivo using several types of porous titanium implants. We concluded that not only high porosity and large pore size but also high interconnectivity of the pores is effective for bone ingrowth and tissue differentiation [23]. Based on this previous study, an optimally structured porous titanium metal was developed and used for this clinical trial. It has 60% porosity, 250 μm average pore size and more than 99% pore interconnectivity.

Another important issue associated with porous metal implants is the difficulty in producing bioactive properties on the inner surfaces of implants using conventional methods such as applying a plasma-sprayed HA coating. In the absence of a bioactive surface, the osteoconductivity of these implants and their capacity to promote fusion is limited. The thickness of a conventional HA coating layer is about 40–50 μm, which cannot be applied to critical supporting structures without changes to surface morphology [5]. Moreover, the conventional HA coating for titanium metal implants has the potential for degradation, absorption and third body wear during long-term implantation, which might be related to its poor clinical results [2, 21]. Our chemical and thermal treatments ensured that bioactive properties were applied to the whole surface of the porous titanium implants without reducing the pore space available for bone ingrowth [15]. Adequate stability of the thin treated layer was confirmed both in vitro and in vivo and might assure the long-term apposition with surrounding bone [9]. This material also offers sufficient resistance to shearing forces during the implantation of treated cementless hip prostheses.

Although titanium metal and its alloys are 'gold standard' materials in orthopedics, one of the potential disadvantages of a metal device is a high elastic modulus. The elastic modulus of solid titanium metal is more than 100 GPa and this will lead to stress shielding around the metal device during long-term implantation. To reduce such a mechanical mismatch between the implant and host

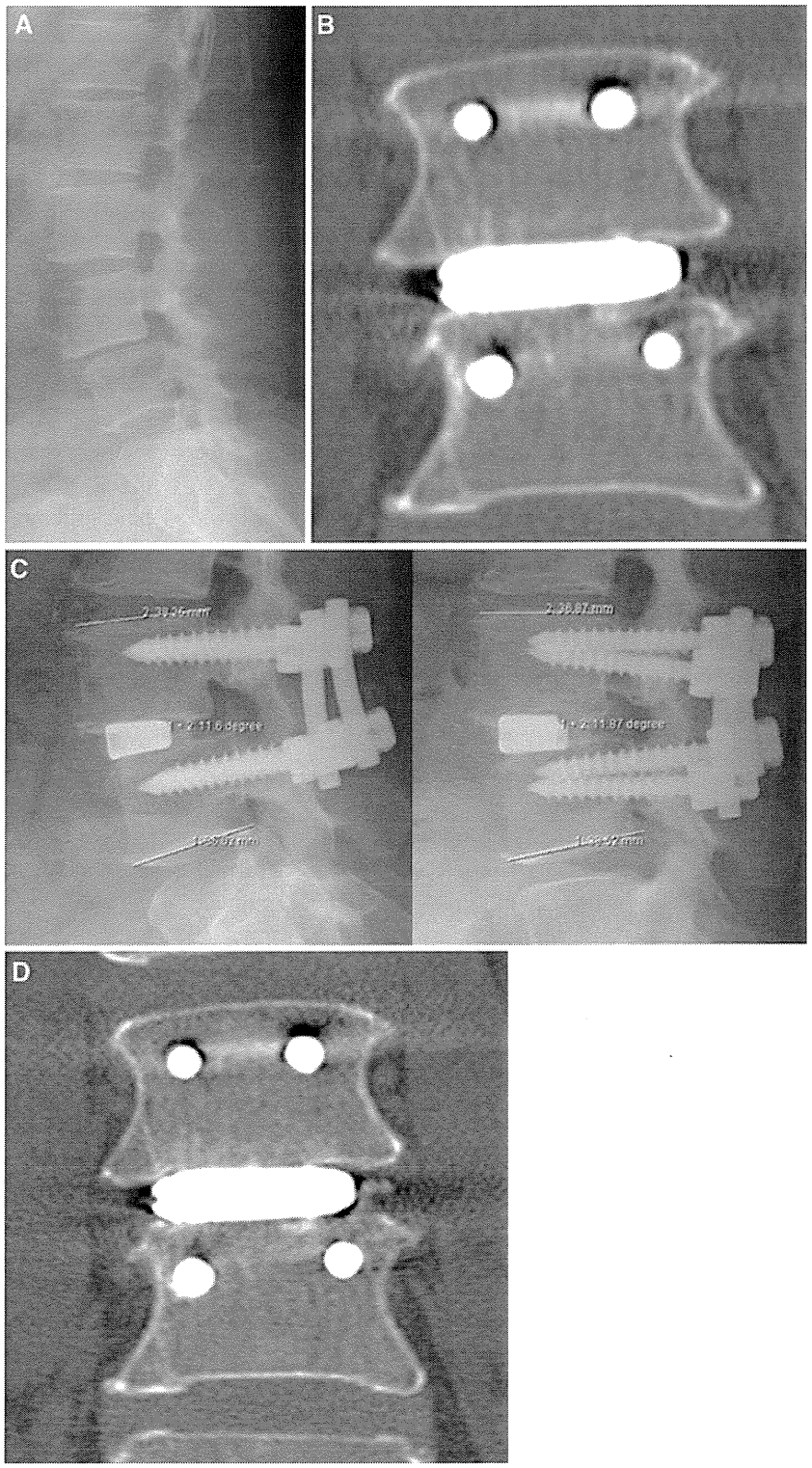

Fig. 6 Preoperative and postoperative radiological studies obtained from a 54-year-old woman with degenerative spondylolisthesis at L4–5 (Case 1). **a** Plain lateral X-ray demonstrating L4 listhesis. **b** Immediate postoperative MDCT image demonstrating a press fit of the porous titanium metal implant to the vertebral endplate. **c** Dynamic lateral radiographs at 3 months showing a solid construct without abnormal segmental motion (*left* flexion; *right* extension). **d** Coronal MDCT image demonstrating solid bony union without device subsidence or any radiolucency at 3 months after surgery

bone, several types of soft material including polyetheretherketone and carbon have been introduced clinically [6, 28]. Although there are no long-term results as yet, porous titanium metal will reduce stress shielding, because the elastic modulus of this material with 60% porosity is 4.2 GPa, close to the value of human cortical bone and much less than solid metal materials. According to Nachemson's study, loads to the human lumbar spine are between 1,000 and 3,000 N during most everyday activities, and increases in different body positions give possible values in excess of 3,000 N during significant lifting [22]. Based upon these data, Brantigan suggested that a lumbar

interbody fusion construct must bear an immediate postoperative load at the bone-implant interface of at least 2,400 N during activities of daily living [4]. On the other hand, breakage of the carbon cage and dissemination of free carbon particles occurred in one case of implant nonunion [29]. A biomechanical study revealed that the carbon cage fractures at around 5,800–8,800 N and concluded that at least 5,000 N was required for an interbody fusion cage [13]. The fatigue strength of porous titanium metal combined with an outer frame is more than 10,000 N under a repetitive compressive load, so it can be used as a spinal interbody fusion device safely.

Another potential disadvantage of a pure metal device is the difficulty of confirming fusion status radiologically because of its high radiodensity. Usually, bony union is confirmed when the following radiological parameters are complete: visible continuous grafted bone trabeculation, no abnormal movement on dynamic study and no radiolucency around the implants. In the case of metal devices such as a titanium cage, bone trabeculation through the cage is difficult to identify on plain X-ray images. However, definitive diagnoses of bony union have become easier with the introduction of MDCT, especially in the case of porous titanium metal, because the metal content is less than with the solid form, recognition of fusion status such as bone-implant interface and bony trabeculation around the implant is not so difficult on MDCT images. In the current study, two specific radiological findings were evident. The first of these was the anchoring effect between the porous bioactive titanium implant and the surrounding vertebral endplate seen on the images taken immediately after surgery. This could be attributed to the optimally rough surface of the porous bioactive device. The second finding was the gap-filling effect. The radiological evidence of gap filling as shown in Fig. 6 resembles the results of alkali- and heat-treated total hip prostheses. Radiological gaps between alkali- and heat-treated metal shells and the acetabulum were filled within 1 year, which indicated the high osteoconductive ability of bioactive titanium metal [14]. The best feature of porous bioactive titanium metal is that it permits bone ingrowth through the inner pore structure. Although we reported good bone ingrowth to the pores in several studies using animal models, we could not confirm this evidence using noninvasive radiological examinations in the present study.

There are some limitations to this study, including its small sample size, short follow-up period and preliminary nature. Our chemical and thermal treatment has been applied clinically for cementless total hip prostheses after a strict clinical trial, which was approved by the Ministry of Health, Labor and Welfare in Japan. Excellent mid-term (4.8 years) clinical results and early bone apposition were reported [14]. These results are encouraging for the efficacy and safety of this surface treatment on titanium and its alloys. Moreover, TLIF is a promising standard procedure for the treatment of patients with unstable spinal disease. Given these encouraging results, we planned this small clinical trial as much as possible to test the efficacy and safety of porous bioactive titanium metal in a spinal fusion device. Fortunately, there was successful bony union without the need for autologous ICBG in this small series. However, implantation of metal devices has a potency to bring about several late complications such as stress shielding and adjacent segment disease during long-term implantation. Therefore, long-term clinical results are mandatory to reveal the true efficacy and safety of this device.

We consider that porous bioactive titanium metal is superior to other porous metal materials in terms of safety, osteoconductive and osteoinductive abilities, mechanical strength and controllable optimum microstructure [10, 24]. Another advantage of porous bioactive titanium metal is its potency for general purpose medical devices. First, our surface treatment can be applied not only to pure titanium but also to several types of titanium alloys. By changing materials, the mechanical characteristics can be optimized. Second, using our manufacturing technique, the pore structure, mechanical strength and biological characteristics can be controlled depending on the conditions. This material will be valuable not only for spinal fusion but also for reconstructive surgery to the skull, the maxillofacial region and in other orthopedic fields. Moreover, adjustments to the elastic modulus and bioactive abilities promise to produce new generations of devices for the treatment of osteoporotic bone.

Conclusions

We developed porous bioactive titanium device for spinal fusion. The optimal mechanical strength and interconnected structure of porous titanium metal were adjusted to the device. The whole surface of porous titanium was treated chemically and thermally to form the bioactive surface. Clinical trial was successfully performed and early bony union was achieved in all cases without ICBG by 6 months. Two specific findings including an anchoring effect and gap filling were evident radiologically. Although a larger and longer-term follow-up clinical study is mandatory to reach any firm conclusions, we consider this porous bioactive titanium metal is promising material for a spinal fusion device.

Acknowledgments The authors thank Hisashi Kitagaki, Tsuneo Teraoka, of Osaka Yakin Co., for manufacturing and providing the porous titanium implants. They thank Seiji Yamaguchi, of Chubu University Biomedical Sciences, for treating the material chemically.

They thank Shuji Higuchi, Masanori Fukushima, Satoshi Teramukai, Kenichi Yoshimura, Toshinori Murayama, Tomoko Yokota, Erika Hirata and Harue Tada, of Kyoto University's translational research center, for help in protocol preparation, moderation of the clinical trial and data management. They also thank Takeshi Sakamoto, Makoto Yoshida and Masahiko Miyata for radiological assessments, and Masato Ota for surgical assistance.

This study was supported by a Grant in Aid for Scientific Research from the Japan Society for the Promotion of Science (No. 19200039). No benefits in any form have been or will be received from a commercial party related directly or indirectly to the subject of this manuscript. This manuscript has not been previously published and is not under consideration for publication elsewhere. The first two authors contributed equally to this study and preparation of this manuscript.

References

1. Banwart JC, Asher MA, Hassanein RS (1995) Iliac crest bone graft harvest donor site morbidity. A statistical evaluation. Spine 20:1055–1060
2. Bloebaum RD, Beeks D, Dorr LD, Savory CG, DuPont J, Hofmann AA (1994) Complications with hydroxyapatite particulate separation in total hip arthroplasty. Clin Orthop 298:19–26
3. Boden SD, Zdeblick TA, Sandu HS, Heim SE (2000) The use of rhBMP-2 in interbody fusion cages: definitive evidence of osteoinduction in humans: a preliminary report. Spine 25:376–381
4. Brantigan JW, Cunningham BW, Warden K, McAfee PC, Steffee AD (1993) Compression strength of donor bone for posterior lumbar interbody fusion. Spine 18:1213–1221
5. De Groot K, Geesink R, Klein CP, Serekian P (1987) Plasma sprayed coatings of hydroxyapatite. J Biomed Mater Res 21: 1375–1381
6. Desogus N, Ennas F, Leuze R et al (2005) Posterior lumbar interbody fusion with PEEK cages: personal experience with 20 patients. J Neurosurg Sci 49:137–141
7. Ducheyne P, Qiu Q (1999) Bioactive ceramics: the effect of surface reactivity on bone formation and bone cell function. Biomaterials 20:2287–2303
8. Fujibayashi S, Shikata J, Tanaka C, Matsushita M, Nakamura T (2001) Lumbar posterolateral fusion with biphasic calcium phosphate ceramic. J Spinal Disord 14:214–221
9. Fujibayashi S, Nakamura T, Nishiguchi S, Tamura J, Uchida M, Kim HM et al (2001) Bioactive titanium: effect of sodium removal on the bone-bonding ability of bioactive titanium prepared by alkali and heat treatment. J Biomed Mater Res 56:562–570
10. Fujibayashi S, Neo M, Kim HM, Kokubo T, Nakamura T (2004) Osteoinduction of porous bioactive titanium metal. Biomaterials 25:443–450
11. Fujibayashi S, Neo M, Takemoto M, Ota M, Nakamura T (2010) Paraspinal-approach transforaminal lumbar interbody fusion for the treatment of lumbar foraminal stenosis. J Neurosurg Spine 13:500–508
12. Hench LL (1998) Bioactive materials: the potential for tissue regeneration. J Biomed Mater Res 41:511–518
13. Jost B, Cripton PA, Lund T, Oxland TR, Lippuner K, Jaeger P et al (1998) Compressive strength of interbody cages in lumbar spine: the effect of cage shape, posterior instrumentation and bone density. Eur Spine J 7:132–141
14. Kawanabe K, Ise K, Goto K, Akiyama H, Nakamura T, Kaneuji A et al (2009) A new cementless total hip arthroplasty with bioactive titanium porous-coating by alkaline and heat treatment: average 4.8-year results. J Biomed Mater Res Part B: Appl Biomater 90B:476–481
15. Kim HM, Kokubo T, Fujibayashi S, Nishiguchi S, Nakamura T (2000) Bioactive macroporous titanium surface layer on titanium substrate. J Biomed Mater Res 52:553–557
16. Kokubo T (1991) Bioactive glass ceramics: properties and applications. Biomaterials 12:155–163
17. Kokubo T, Kushitani H, Sakka S, Kitsugi T, Yamamuro T (1990) Solutions able to reproduce in vivo surface-structure changes in bioactive glass-ceramic A-W. J Biomed Mater Res 24:721–734
18. Kokubo T, Miyaji F, Kim HM, Nakamura T (1996) Spontaneous formation of bonelike apatite layer on chemically treated titanium metals. J Am Ceram Soc 79:1127–1129
19. McClellan JW, Mulconrey DS, Forbes RJ, Fullmer N (2006) Vertebral bone resorption after transforaminal lumbar interbody fusion with bone morphogenetic protein (rhBMP-2). J Spinal Disord Tech 19:483–486
20. Modic MT, Steinberg PM, Ross JS, Masaryk TJ, Carter JR (1988) Degenerative disk disease: assessment of changes in vertebral body marrow with MR imaging. Radiology 166:193–199
21. Morscher EW, Hefti A, Aebi U (1998) Severe osteolysis after third body wear due to hydroxyapatite particles from acetabular cup coating. J Bone Joint Surg Br 80:267–272
22. Nachemson AL (1981) Disc pressure measurements. Spine 6:93–97
23. Otsuki B, Takemoto M, Fujibayashi S, Neo M, Kokubo T, Nakamura T (2006) Pore throat size and connectivity determine bone and tissue ingrowth into porous implants: three-dimensional micro-CT based structural analyses of porous bioactive titanium implants. Biomaterials 27:5892–5900
24. Takemoto M, Fujibayashi S, Neo M, Suzuki J, Kokubo T, Nakamura T (2005) Mechanical properties and osteoconductivity of porous bioactive titanium. Biomaterials 26:6014–6023
25. Takemoto M, Fujibayashi S, Neo M, Suzuki J, Matsushita T, Kokubo T, Nakamura T (2006) Osteoinductive porous titanium implants: effect of sodium removal by dilute HCl treatment. Biomaterials 27:2682–2691
26. Takemoto M, Fujibayashi S, Neo M, So K, Akiyama N, Matsushita T et al (2007) A porous bioactive titanium implant for spinal interbody fusion: an experimental study using a canine model. J Neurosurg Spine 7:435–443
27. Toth JM, Boden SD, Burkus JK MD, Badura JM, Peckham SM, McKay WF (2009) Short-term osteoclastic activity induced by locally high concentrations of recombinant human bone morphogenetic protein-2 in a cancellous bone environment. Spine 34:539–550
28. Tullberg T, Brandt B, Rydberg J, Fritzell P (1996) Fusion rate after posterior lumbar interbody fusion with carbon fiber implant: 1-year follow-up of 51 patients. Eur Spine J 5:178–182
29. Tullberg T (1998) Failure of a carbon fiber implant: a case report. Spine 23:1804–1806
30. Vaccaro AR, Lawrence JP, Patel T, Katz LD, Anderson DG, Fischgrund JS et al (2008) The safety and efficacy of OP-1 (rhBMP-7) as a replacement for iliac crest autograft in posterolateral lumbar arthrodesis. Spine 33:2850–2862
31. Vaidya R, Sethi A, Bartol S, Jacobson M, Coe C, Craig JG (2008) Complications in the use of rhBMP-2 in PEEK cages for interbody spinal fusions. J Spinal Disord Tech 21:557–562
32. Wen CE, Mabuchi M, Yamada Y, Shimojima K, Chino Y, Asahina T (2001) Processing of biocompatible porous Ti and Mg. Scripta Mater 45:1147–1153

ELSEVIER

Experimental Hematology

Experimental Hematology 2011;39:424–433

Cross-priming of CD8$^+$ T cells in vivo by dendritic cells pulsed with autologous apoptotic leukemic cells in immunotherapy for elderly patients with acute myeloid leukemia

Toshio Kitawaki[a], Norimitsu Kadowaki[a], Keiko Fukunaga[a], Yasunari Kasai[b], Taira Maekawa[b], Katsuyuki Ohmori[c], Tatsuya Itoh[d], Akira Shimizu[d], Kiyotaka Kuzushima[e], Tadakazu Kondo[a], Takayuki Ishikawa[a], and Takashi Uchiyama[a]

[a]*Department of Hematology and Oncology;* [b]*Center for Cell and Molecular Therapy, Department of Transfusion Medicine and Cell Therapy;* [c]*Department of Clinical Laboratory Medicine;* [d]*Department of Experimental Therapeutics, Kyoto University Hospital, Kyoto, Japan;* [e]*Division of Immunology, Aichi Cancer Center Research Institute, Nagoya, Japan*

(Received 11 November 2010; revised 28 December 2010; accepted 1 January 2011)

Objective. **The prognosis for elderly patients with acute myeloid leukemia (AML) remains dismal. To explore the potential of immunotherapy for improving clinical outcomes for these patients, we performed a phase I clinical trial of dendritic cell (DC)–based immunotherapy for elderly patients with AML.**

Materials and Methods. **Autologus monocytes were obtained after reducing tumor burden by chemotherapy. Immature DCs induced with granulocyte-macrophage colony-stimulating factor and interleukin-4 were pulsed with autologous apoptotic leukemic cells as antigens. DCs were administered intradermally to four patients five times at 2-week intervals. To facilitate DC migration to lymph nodes, injection sites were pretreated with killed *Streptococcus pyogenes* OK-432 one day before. DCs were coinjected with OK-432 to induce maturation and interleukin-12 production in vivo.**

Results. **Antileukemic responses were observed by an interferon-γ enzyme-linked immunospot assay or a tetramer assay in two of four patients. In a human leukocyte antigen–A*2402-positive patient, induction of CD8$^+$ T-cell responses to WT1- and human telomerase reverse transcriptase–derived peptides were observed, indicating cross-priming in vivo. The two patients with antileukemic immunity showed longer periods of disease stabilization than the other two patients.**

Conclusions. **This study demonstrates the immunogenicity of autologous DCs that cross-present leukemia-associated antigens from autologous apoptotic leukemic cells in vivo in elderly patients with AML.**

Management of elderly patients with acute myeloid leukemia (AML) remains a challenge because of a high rate of therapy-related mortality and chemotherapy resistance [1]. Antigen-specific immunotherapy, which is less toxic and kills leukemic cells through different mechanisms than chemotherapy, has the potential capacity to improve the clinical outcomes of these patients. Recent identification of several leukemia-associated antigens prompted us to develop immunotherapy for elderly patients with AML [2].

Active immunization by peptide vaccines can induce antileukemic immunity and clinical responses in AML [3–6]. Clinical trials of dendritic cell (DC)–based immunotherapy for AML have also been reported [7–12]. However, the trial using leukemic cell–derived DCs showed that the generation of leukemic cell–derived DCs was feasible in only a limited number of patients, and even in vaccinated patients the treatment could not induce clinical responses [9]. This may be due to lower immunostimulatory activity of leukemic cell–derived DCs than monocyte-derived DCs (MoDCs) [13]. Recently, the efficient generation of MoDCs from patients with AML has been demonstrated in vitro [14], providing a rationale for the use of MoDCs in immunotherapy for AML.

Offprint requests to: Norimitsu Kadowaki, M.D., Ph.D., Department of Hematology and Oncology, Graduate School of Medicine, Kyoto University, 54 Shogoin Kawara-cho, Sakyo-ku, Kyoto 606-8507, Japan; E-mail: kadowaki@kuhp.kyoto-u.ac.jp

Supplementary data associated with this article can be found in the online version at doi:10.1016/j.exphem.2011.01.001.

0301-472X/$ - see front matter.
doi: 10.1016/j.exphem.2011.01.001

There are several parameters to enhance the immunogenicity of MoDC vaccines. Whereas monocytes are cultured with granulocyte-macrophage colony-stimulating factor (GM-CSF) and interleukin (IL)-4 conventionally for 5 to 7 days to induce DCs, a shorter period of culture is sufficient to induce equivalently potent DCs [15]. Among DC maturation–inducing factors, microbial components that trigger the production of IL-12 are beneficial to induce effective adaptive immunity [16]. An extended period of stimulation with microbial components results in DC exhaustion in which DCs lose the capacity to produce IL-12 [17]. Thus, a short-term stimulation can generate optimal DCs that retain IL-12 production. Inflammation in the skin before DC injection facilitates DC migration to draining lymph nodes, leading to a stronger immune response [18,19]. Using apoptotic whole tumor cells as antigens may be instrumental in inducing multivalent immune responses [20].

We performed in vitro assays to optimize these parameters. Based on the results of these assays, we conducted a phase I clinical trial of immunotherapy for elderly patients with AML at the second or later remission setting, using DCs loaded with autologous apoptotic leukemic cells. The treatment was well-tolerated and safe and induced antileukemic immunity in two of four patients, which was associated with transient disease stabilization. Importantly, in one patient, cross-priming of leukemia antigen–specific $CD8^+$ T cells in vivo was explicitly demonstrated. This study indicates the safety and immunogenicity of immunotherapy using MoDCs that cross-present leukemic cell antigens in elderly patients with AML.

Materials and methods

Generation, maturation, and cryopreservation of DCs for in vitro assays

Peripheral blood mononuclear cells (PBMCs) were obtained from healthy volunteers by density gradient centrifugation using Lympholyte H (Cedarlane, Ontario, Canada). Monocytes were purified using anti–CD14-conjugated microbeads (Miltenyi Biotec, Bergisch Gladbach, Germany), or enriched by plastic adherence by incubating PBMCs at 37°C for 2 hours and removing nonadherent cells by pipetting. Monocytes were cultured with 800 IU/mL GM-CSF (Primmune, Kobe, Japan) and 500 IU/mL IL-4 (Primmune) in CellGro DC medium (CellGenix Technologie Transfer, Freiburg, Germany) for 3 days (3d-DCs) or 6 days (6d-DCs). In some experiments, 3d-DCs were frozen in CP-1 freezing medium (Kyokuto Pharmaceutical Industrial, Tokyo, Japan). CP-1 contains 12% hydroxymethyl starch and 10% dimethyl sulfoxide in normal saline and was mixed with 8% human serum albumin before use. DCs were matured with 0.1 KE/mL OK-432 (Picibanil; Chugai Pharmaceuticals, Tokyo, Japan), a penicillin-killed and lyophilized preparation of a low-virulence strain (Su) of *Streptococcus pyogenes* (group A) [21].

In vitro analysis of DC functions

Flow cytometric analysis, measurement of IL-12p70 production, T-cell–stimulatory capacity of DCs for allogeneic naive $CD4^+$ T cells, and the cytokine profile of $CD4^+$ T cells primed with DCs were analyzed as described previously [15,22].

Uptake of apoptotic cells by DCs and the cross-presenting capacity of DCs

Efficiency of uptake of apoptotic cells by DCs was assessed as described previously [23] using myeloid leukemia cell lines K562, OUN-1 [24] (Dr. Yasukawa, Ehime University, Japan), and a T-cell leukemia cell line MT2, which were killed by 120 Gy γ-irradiation and 48-hour serum-free culture in RPMI-1640 (Wako Pure Chemical Industries, Osaka, Japan). To examine the cross-presenting capacity of DCs, human leukocyte antigen (HLA)-A*2402–positive, immature 3d-DCs were pulsed with HLA-A*2402–negative, Epstein-Barr virus–transformed lymphoblastoid cell lines, which were killed as described here. DCs were matured with OK-432 (0.1 KE/mL) and prostaglandin E_2 (1 μg/mL) (MP Biomedicals, Solon, OH, USA) for 6 hours, and cocultured with autologous T cells at a DC-to-T cell ratio of 1:10. IL-2 (50 IU/mL; Teceleukin; Shionogi & Co., Ltd., Osaka, Japan) was added on the next day. For a positive control, DCs pulsed with HLA-A*2402–restricted EBNA3B peptide (TYSAGIVQI; KURABO Industries, Osaka, Japan) were used. Expansion of EBNA3A- and EBNA3B-specific $CD8^+$ T cells were evaluated by HLA tetramer staining [25].

Clinical trial protocol

The protocol was approved by the Ethics Committee, Graduate School and Faculty of Medicine, Kyoto University. Each patient gave written informed consent in accordance with the Declaration of Helsinki. The primary and secondary objectives were the assessment of safety and immunological and clinical responses, respectively.

Autologous leukemic cells were harvested before induction chemotherapy. Patients were required to be between 16 and 79 years of age and have a diagnosis of AML according to World Health Organization criteria [26,27]. Patients were excluded if they had another concurrent malignancy, an active autoimmune disease, positivity for blood-borne infectious agents, or a history of penicillin allergy (because OK-432 contains penicillin). Patients were enrolled if 5×10^7 or more leukemic cells were harvested. Thereafter, patients were treated with chemotherapy. More than 4 weeks after the last chemotherapy, patients proceeded to the DC vaccination if leukemic cells in bone marrow (BM) were $<20\%$. In addition, to assess the clinical efficacy of DC vaccination, the presence of an evaluable lesion in BM, which was defined as 0.1% or more of leukemic cells by flow cytometry, was required. Furthermore, patients should have an Eastern Cooperative Oncology Group performance status of 0 to 2 and adequate vital organ functions. Patients were excluded if they had eligibility for hematopoietic stem cell transplantation or an uncontrollable infection. Concomitant chemotherapy and radiotherapy were prohibited.

DC vaccine generation

DC vaccines were generated from autologous monocytes under current Good Manufacturing Practice conditions. Autologous leukemic cells to be used as antigens were obtained as mononuclear cells (MNCs) by density gradient centrifugation over Ficoll-Hypaque (GE Healthcare, Buckinghamshire, UK) from BM and/or peripheral blood (PB) samples. MNCs were frozen in CP-1 freezing medium and stored at −150°C. Before added to DCs, MNCs were killed by 120 Gy

γ-irradiation and 48 hours serum starvation. Killing of MNCs was confirmed by the percentage of Annexin V–positive cells being 90% or more by flow cytometry and reduced uptake of [^{3}H]-thymidine to the baseline level.

Apheresis products, which were obtained with COBE Spectra (Caridian BCT, Lakewood, CO, USA) from 10 L blood, were processed by elutriation using Elutra (Caridian BCT) to enrich monocytes. At the time of apheresis, no leukemic cells were observed in the PB of the patients, as assessed by a routine clinical laboratory test. Monocytes were cultured with 800 U/mL GM-CSF and 500 U/mL IL-4 in CellGro DC medium in gas-permeable plastic bags (VueLife 118; CellGenix Technologie Transfer) at 37°C, 5% CO_2 to generate immature DCs. After 48 hours, DCs were pulsed with autologous apoptotic leukemic cells and 2 μg/mL keyhole-limpet hemocyanin (KLH; Biosyn Corporation, Carlsbad, CA, USA). The endotoxin level in the KLH preparation examined by the supplier was <0.1 IU/mg. After an additional 24 hours, DCs were frozen as immature DCs in CP-1 freezing medium and stored at −150°C.

Administration of the DC vaccine

A total of 1×10^7 DCs were intradermally injected at four sites in bilateral arms and thighs. Twenty-four hours before DC administration, the injection sites were pretreated by 0.2 KE/site OK-432. At the time of DC administration, DCs were thawed and mixed with 1 KE OK-432. Then, the mixture of DCs and OK-432 was injected. The DC administration was repeated at 2-week intervals for five administrations.

Monitoring of immunological and clinical responses

Antigen-specific immune responses were assessed at indicated time points. Immune responses to KLH and autologous leukemic cells were tested by skin delayed-type hypersensitivity tests and interferon (IFN)-γ enzyme-linked immunospot (ELISPOT) assays. In addition, in a HLA-A*2402–positive patient, immune responses to HLA-A*2402–restricted peptides derived from leukemia-associated antigens were examined by IFN-γ ELISPOT assay and HLA tetramer staining. The peptides used in the assays were the natural $WT1_{235-243}$ peptide (CMTWNQMNL) [24], the modified $WT1_{235-243}$ peptide (CYTWNQMNL) [28], the human telomerase reverse transcriptase $(hTERT)_{461-469}$ peptide (VYGFVRACL) [29], and the lower matrix 65-kd phosphoprotein (pp65) of cytomegalovirus (CMV) (amino acids 328–336; QYDPVAALF) [30]. All peptides were purchased from Multiple Peptide Systems (San Diego, CA, USA). Both PBMCs and BM mononuclear cells (BMMCs) were subjected to assays before and after 1-week in vitro stimulation with antigen- or peptide-pulsed DCs in the presence of 15 U/mL IL-2 (Teceleukin). To evaluate clinical responses, percentages of leukemic cells in BM were monitored by morphology and flow cytometry at indicated time points.

Skin delayed-type hypersensitivity test

The 4×10^5 antigen-pulsed DCs were intradermally injected in the forearm. Sizes of induration and erythema were measured 48 hours later. Erythema that was 1.5-fold or larger in diameter than the antigen-unpulsed control was considered positive.

IFN-γ ELISPOT assay

IFN-γ ELISPOT assays (Mabtech, Nacka Strand, Sweden) were performed using antigen-pulsed DCs and peptide-pulsed C1R-A*2402 (Dr. Masafumi Takiguchi, Kumamoto University, Kumamoto, Japan). Stimulator cells were plated at 2×10^4 cells/well. As responder cells, fresh and in vitro–stimulated MNCs from PB and BM were plated with fresh MNCs at 1 to 2×10^5 cells/well and in vitro–stimulated MNCs at 1 to 2×10^4 cells/well. After overnight incubation, spots were developed using 3-amino-9-ethylcarbazole (Sigma Chemical, St Louis, MO, USA) and counted by KS ELISPOT compact (Carl Zeiss MicroImaging, Tokyo, Japan). Numbers of specific spot-forming cells were calculated by subtracting the number of spots with unpulsed DCs from the number of spots with antigen-pulsed DCs.

HLA tetramer staining

Natural $WT1_{235-243}$ peptide/HLA-A*2402 tetramer was purchased from Medical & Biological Laboratories (Nagoya, Japan). Modified $WT1_{235-243}$ peptide/HLA-A*2402 tetramer and a peptide derived from the HIV envelope (env) protein/HLA-A*2402 tetramer were produced as described previously [30]. Fresh and in vitro–stimulated MNCs were stained with a tetramer and fluorescein isothiocyanate–conjugated anti-CD8 monoclonal antibody (BD Biosciences) and analyzed by flow cytometery (FACSCalibur; BD Biosciences) [30].

Results

In vitro assays to optimize generation of DCs

To optimize generation of DCs, we performed in vitro functional assays. We first compared DCs differentiated from monocytes in the presence of GM-CSF and IL-4 for 3 days with 6-day differentiated DCs conventionally used in clinical trials. After 24-hour exposure to OK-432, both 3d-DCs and 6d-DCs showed similar levels of surface molecule expressions, IL-12p70 production, and T-cell stimulatory capacity for allogeneic naïve $CD4^+$ T cells (Supplementary Figure E1; online only, available at www.exphem.org), indicating that 3d-DCs have functions comparable with 6d-DCs. Next, we examined the capacity of 3d-DCs to cross-present apoptotic cell–associated antigens. At the DC-to-apoptotic cell ratio of 1:1, 11% to 33% of immature 3d-DCs incorporated apoptotic leukemia cell lines (Fig. 1A). Moreover, HLA-A*2402–positive DCs pulsed with killed lymphoblastoid cell lines from an HLA-A*2402–negative donor induced expansion of $CD8^+$ T cells specific for the HLA-A*2402–restricted epitopes of EBNA3A and EBNA3B (Fig. 1B), indicating the capacity of DCs to cross-present apoptotic cell–derived antigens.

An extended period of exposure of DCs to lipopolysaccharide leads to DC exhaustion [17], as indicated by loss of IL-12–producing capacity by DCs. To examine whether OK-432 induces DC exhaustion, we analyzed the maturation kinetics of OK-432–stimulated 3d-DCs. Upregulation of the surface molecules (Fig. 2A) and IL-12p70 production (Fig. 2B) became evident 4 and 8 hours after OK-432 stimulation, respectively. Maximal levels of surface molecule expressions and IL-12p70 production were observed at 48 hours. Next, we examined how many hours of exposure to OK-432 is sufficient to elicit a maturation signal to DCs, using 3d-DCs that were cultured for a total of 48 hours with different

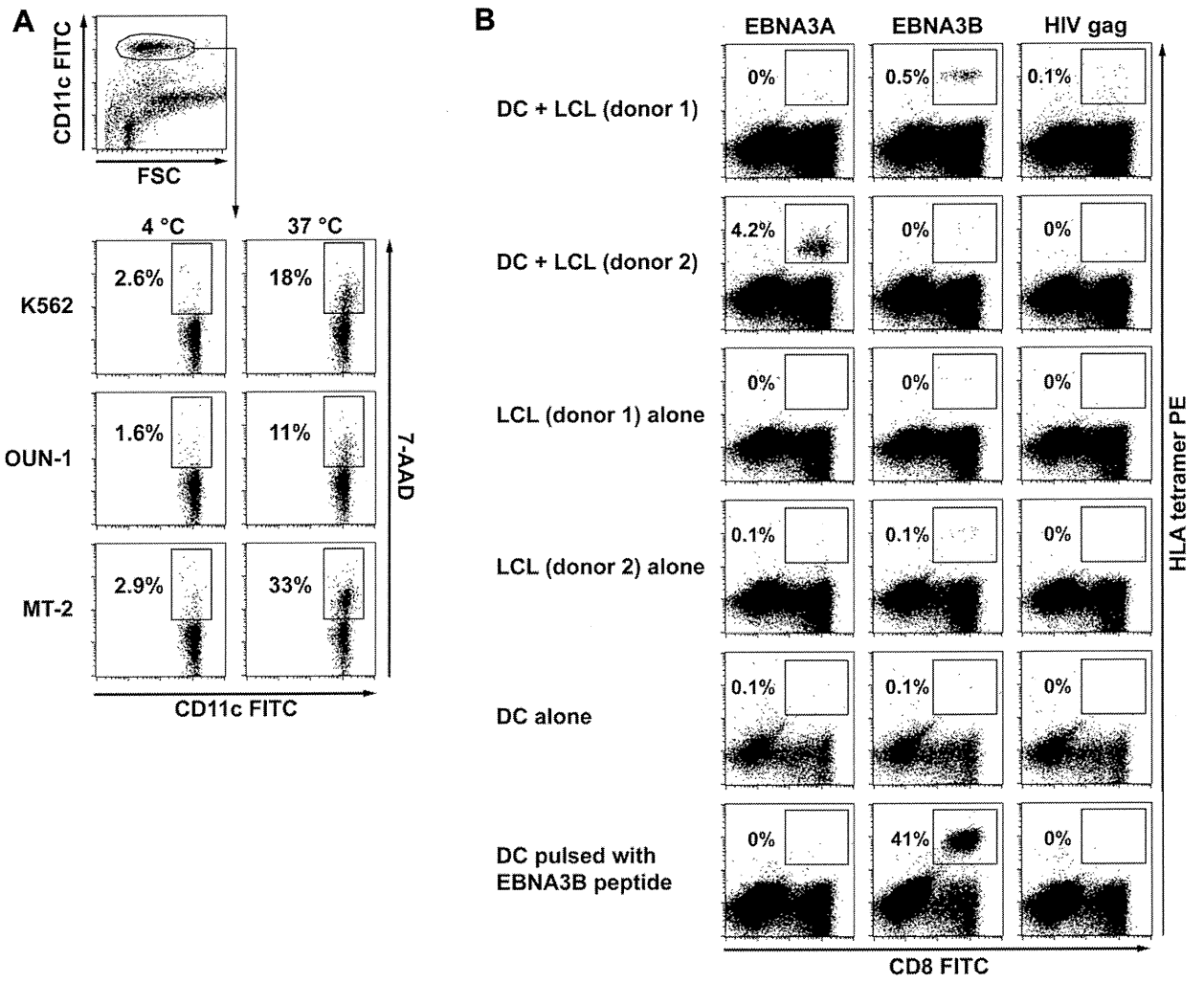

Figure 1. 3d-DCs incorporate apoptotic cells and cross-present cell-associated antigens. (**A**) Uptake of apoptotic cells by 3d-DCs. Apoptotic K562, OUN-1, and MT2 were labeled with 7-aminoactinomycin D (7-AAD) (20 μg/mL), and cocultured with immature 3d-DCs at a DC-to-apoptotic cell ratio of 1:1. After 4 hours of incubation at 4°C or 37°C, cells were stained with fluorescein isothiocyanate–conjugated anti-CD11c monoclonal antibody and analyzed by flow cytometry. Cells positive for both CD11c and 7-AAD were considered to be DCs that had phagocytosed apoptotic cells. (**B**) The cross-presenting capacity of DCs. Immature 3d-DCs from a HLA-A*2402–positive donor were pulsed with apoptotic HLA-A*2402–negative donor-derived lymphoblastoid cell lines (LCLs), matured with OK-432 and prostaglandin E_2, and cocultured with autologous T cells. For a positive control, DCs pulsed with the EBNA3B peptide were used as a stimulator. After 7 days, expansions of EBNA3A- and EBNA3B-specific $CD8^+$ T cells were evaluated by HLA tetramer staining. Dead cells are excluded by staining with propidium iodide. Numbers shown indicate percentages of tetramer-positive cells among $CD8^+$ cells. Representative data from two experiments are shown.

durations of exposure to OK-432 at the start of culture. As short as 2-hour exposure upregulated CD83 and CD86 (Fig. 2C) and induced IL-12p70 production (Fig. 2D) during the subsequent 46-hour culture without OK-432. Although at the time of 8-hour exposure, the induction of CD83, CD86 (Fig. 2A), and IL-12p70 (Fig. 2B) was low, 8-hour exposure was sufficient to induce maximal levels of CD83 and CD86 expression (Fig. 2C) and IL-12p70 production (Fig. 2D). Notably, although initial 24-hour exposure to OK-432 induced the maximal levels of CD83 and CD86 expression (Fig. 2C), DCs did not produce a detectable level of IL-12p70 during the last 24-hour culture (Fig. 2D). These data indicate that, like lipopolysaccharide [17], OK-432–induced IL-12p70 production was limited within the first 24 hours and most active between 8 and 24 hours after OK-432 stimulation. The functional significance of ongoing IL-12p70 production by DCs in priming naïve $CD4^+$ T cells was supported by the data that 3d-DCs matured with OK-432 for 6 hours showed a superior capacity to induce IFN-γ–producing T cells to those matured for 24 hours (Fig. 2E). Thus, extended stimulation with OK-432 induces DC exhaustion. To avoid it, we decided to administer immature DCs together with OK-432 to patients and to induce DC maturation in vivo.

It is convenient to prepare a large number of DCs from a single batch of apheresis and freeze them in aliquots. We assessed the effect of cryopreservation on DCs. Whereas cryopreserved immature 3d-DCs showed somewhat higher percentages of dead cells after 24-hour culture with or